



HAL
open science

Simulation of electrified storms with comparison of the charge structure and lightning efficiency

Christelle Barthe, Jean-Pierre Pinty

► **To cite this version:**

Christelle Barthe, Jean-Pierre Pinty. Simulation of electrified storms with comparison of the charge structure and lightning efficiency. *Journal of Geophysical Research: Atmospheres*, 2007, 112, pp.D19204. 10.1029/2006JD008241 . hal-00564809

HAL Id: hal-00564809

<https://hal.science/hal-00564809>

Submitted on 16 Jun 2022

HAL is a multi-disciplinary open access archive for the deposit and dissemination of scientific research documents, whether they are published or not. The documents may come from teaching and research institutions in France or abroad, or from public or private research centers.

L'archive ouverte pluridisciplinaire **HAL**, est destinée au dépôt et à la diffusion de documents scientifiques de niveau recherche, publiés ou non, émanant des établissements d'enseignement et de recherche français ou étrangers, des laboratoires publics ou privés.

Copyright

Simulation of electrified storms with comparison of the charge structure and lightning efficiency

Christelle Barthe¹ and Jean-Pierre Pinty¹

Received 10 November 2006; revised 12 March 2007; accepted 17 July 2007; published 12 October 2007.

[1] An electrification and lightning flash scheme was run in a cloud-resolving model to study the electrical structure of idealized convective storms with several charge separation parameterizations. The electrification of an intense multicellular storm was first simulated. The results confirm the sensitivity of the cloud polarity and lightning flash characteristics to three noninductive charging formulations. Furthermore, it is found that the inductive charging is an efficient mechanism to enhance the lower electric charge, which favors cloud-to-ground flashes. Then, microphysical and electrical budgets were calculated for the convective and stratiform regions of a two-dimensional squall line. The simulation shows that the liquid water content is high enough to generate graupel by riming. Thus the noninductive separation process is efficient to charge the stratiform plume as well, and lightning flashes can be triggered. Finally, the application of various noninductive charging schemes to several convective storms showed the storm electrification variability, which heavily depends on the cloud dynamics and microphysics. The study reveals some remarkable features concerning the charge structure and the cloud-to-ground flash polarity.

Citation: Barthe, C., and J.-P. Pinty (2007), Simulation of electrified storms with comparison of the charge structure and lightning efficiency, *J. Geophys. Res.*, 112, D19204, doi:10.1029/2006JD008241.

1. Introduction

[2] The concomitant dynamical, microphysical, and purely electrical aspects of deep convection is currently a source of perplexity, especially when one attempts to unravel and to simulate the mechanisms responsible for sustained electrical activity inside thunderstorms [Ziegler *et al.*, 1986; MacGorman and Burgess, 1994; Lang and Rutledge, 2002; Carey *et al.*, 2003; MacGorman *et al.*, 2005]. At present, the occurrence, the polarity, and the frequency of lightning flashes can still be considered as one of the most unpredictable features among short-range atmospheric events.

[3] In numerical models, a potential source of uncertainty comes from the mixed-phase microphysical schemes. They quantify the growth of the condensate and all the possible collection rates between cloud particles and hydrometeors. Even with some evidence that cloud-resolving models can simulate the amount of precipitation at high resolution with some confidence [Stoelinga *et al.*, 2003; Walser *et al.*, 2004; Colle *et al.*, 2005], little is known about the capability of these mixed-phase microphysical schemes to treat the charge separation and charge transfer mechanisms which are at the origin of electrical activity inside the storms. In addition, according to recent views, the triggering and the propagation of lightning discharges themselves have a probabilistic nature to some degree [Mansell *et al.*, 2002;

Barthe *et al.*, 2005]. This means that interpreting lightning flash characteristics (location, frequency, type, strength, etc.) as an index of severity of deep convection or as an indicator of storm maturity [Zipser and Lutz, 1994; Toracinta *et al.*, 2002; Cecil *et al.*, 2005; Prigent *et al.*, 2005] is definitely a difficult task. It would therefore be worthwhile to try to obtain more insights in electrification models by exploring idealized test cases using an electric charge cycle scheme [Helsdon *et al.*, 2001; Mansell *et al.*, 2005; Altaratz *et al.*, 2005], here coupled to an original lightning scheme [Barthe *et al.*, 2005; Barthe and Pinty, 2007].

[4] Besides the dynamical and microphysical contributions to the poorly determined electrical state of thunderstorms, the numerical representation of the electrification processes is a matter of debate. Extensive studies agree now that the noninductive process is the leading charging process in clouds. However, the physics of this mechanism is not firmly established despite recent progress [Dash *et al.*, 2001; Nelson and Baker, 2003]. So existing parameterizations rely solely on meticulous laboratory measurements [Takahashi, 1978; Jayaratne *et al.*, 1983; Saunders *et al.*, 1991; Saunders and Peck, 1998; Pereyra *et al.*, 2000]. A common finding of these laboratory experiments is that noninductive charge separation rates depend on the temperature, the liquid water content, the relative vertical velocity, and the crystal diameter. However, because of different experimental designs, substantially different parameterizations have been published for the amplitude and even the sign of the quantity of charge exchanged at a given temperature and liquid water content. In the Takahashi

¹Laboratoire d'Aérodynamique, Université Paul-Sabatier and CNRS, Toulouse, France.

[1978] parameterization and for temperatures warmer than -10°C , the graupel always charges positively, while for temperatures colder than -10°C , the charge separated depends on the liquid water content. Concerning Saunders's parameterizations [Saunders *et al.*, 1991; Saunders and Peck, 1998], a positive charge is transferred to the graupel for high liquid water content and warm temperature, and the charge gained by the graupel is negative in the case of low liquid water content and cold temperature. As a result, the variability between the parameterizations is strong enough for different electrical evolutions to be expected and simulated for the same thunderstorm [Helsdon *et al.*, 2001; Mansell *et al.*, 2005; Altaratz *et al.*, 2005].

[5] Helsdon *et al.* [2001] reviewed the merits of the noninductive parameterizations by Takahashi [1978, hereinafter referred to as T78] and Saunders *et al.* [1991, hereinafter referred to as S91]. The two-dimensional (2-D) storm electrification model [Helsdon and Farley, 1987] was used to simulate a Montana thunderstorm up to the first triggered flash. This showed that T78 and S91 led to a direct and an inverse electric dipole formation, respectively. In the case of S91, they found that for low liquid water content, the charge exchange rate was too high and suggested a reduction in the charge transfer values in this region. Altaratz *et al.* [2005] introduced a cloud electrification scheme in the 3-D RAMS model but without a lightning scheme. Comparisons between T78 and S91 were conducted on a wintertime Mediterranean thunderstorm. The results agreed with previous studies. They showed that T78 tended to produce a tripolar charge distribution, while S91 produced an inverted dipole. Mansell *et al.* [2005] performed the most complete numerical study of cloud electrification. Their three-dimensional (3-D) cloud model [Mansell *et al.*, 2002] was used to test different parameterizations of the electrification processes and their influence on the cloud electrical structure and lightning activity. They concluded that the inductive mechanism became significant when used in complement to the noninductive process and that the formation of a normal versus inverted polarity structure was a strong distinguishing feature between T78 and S91. A common feature of these studies is that they focused on a single convective event each time. In contrast, this paper investigates different convective cases with the same electrification scheme to obtain a more general characterization of the different regimes of charge separation and to measure their impact on lightning activity. The charge separation rate is strongly dependent on the temperature and the liquid water content. Therefore the electrical structure of the storms does not depend only on the electrification parameterization itself. It is also related to the cloud dynamics and to the cloud microphysics, which is explained by the high sensitivity of the strength and polarity of electrified structures in the storms to the supercooled water.

[6] Several test cases were studied using the electrification and lightning flash schemes described in Barthe *et al.* [2005] and Barthe and Pinty [2007]. First, the study of the electrification of the multicellular storm described by Mansell *et al.* [2002, 2005] was repeated but at a coarser resolution. Second, a two-dimensional experiment was performed for a long-lasting tropical squall line [Caniaux *et al.*, 1994]. The approximate steadiness of the organized

mesoscale flow allowed the charge budgets to be computed for the first time. Finally, the electrification of different convective events (squall line, supercell, and multicell) was reexamined. The sensitivity of the charge structure and the flash type and frequency to the charge separation mechanisms was investigated. The study concludes with some perspectives about the simulation of electrified storms at kilometer-scale resolution.

2. Summary of the Electrical Scheme

[7] The electrical scheme was developed in the French mesoscale model Méso-NH [Lafore *et al.*, 1998]. The details can be found in the work of Barthe *et al.* [2005] and Barthe and Pinty [2007], so only a brief summary is given in this section.

[8] The electric charges are carried by five categories of hydrometeors (cloud droplets, raindrops, pristine ice, snow, and graupel). The complete life cycle of the electric charges is described in the model with the charge separation, transfer, and transport, and the charge neutralization by lightning flashes. First, electric charges are separated by the noninductive mechanism, for which different parameterizations are available in the model: Takahashi [1978], Saunders *et al.* [1991], and Saunders and Peck [1998] but including some of the modifications suggested by Mansell *et al.* [2005] and hence referred to as M05. The noninductive charging mechanism is the result of elastic collisions between ice particles with a different degree of riming and in the presence of supercooled water. Once an intense electric field of a few tens of kilovolts per meter is generated in the cloud, the inductive process may become efficient and so it should be accounted for. The inductive process is parameterized following Ziegler *et al.* [1991] and deals with elastic collisions between cloud droplets and graupel.

[9] Once electric charges are separated, they are transferred from particle type to particle type during the microphysical conversion processes (aggregation, autoconversion, melting. . .). At the same time, the charges are transported by sedimentation, advection and turbulence. When the in-cloud electric field becomes higher than an altitude-dependant threshold [Marshall *et al.*, 1995], a lightning flash is triggered. The first stage of the flash consists of a bidirectional leader [Kasemir, 1960, 1983]. It propagates upstream and downstream along the electric field until the value falls below a propagation threshold. A branching scheme is then added to reproduce the coarse grain tortuosity and the multiple branches of natural lightning flashes. The scheme is based on the dielectric breakdown model of Niemeyer *et al.* [1984] which represents the growing structure of the lightning path satisfactorily. An iterative algorithm computes and places the branch segments. The number of branches follows a fractal law of distance from the initial triggering point. Branches are allowed to propagate only in regions where the electric field is low but the charge density is high enough [MacGorman *et al.*, 2001]. Cloud-to-ground are treated in an artificial way. They are extended to the ground when a downward segment reaches a threshold altitude (typically 2 km). Finally, the electric charges are partially neutralized along the lightning flash path following Ziegler and MacGorman [1994] and MacGorman *et al.* [2001].

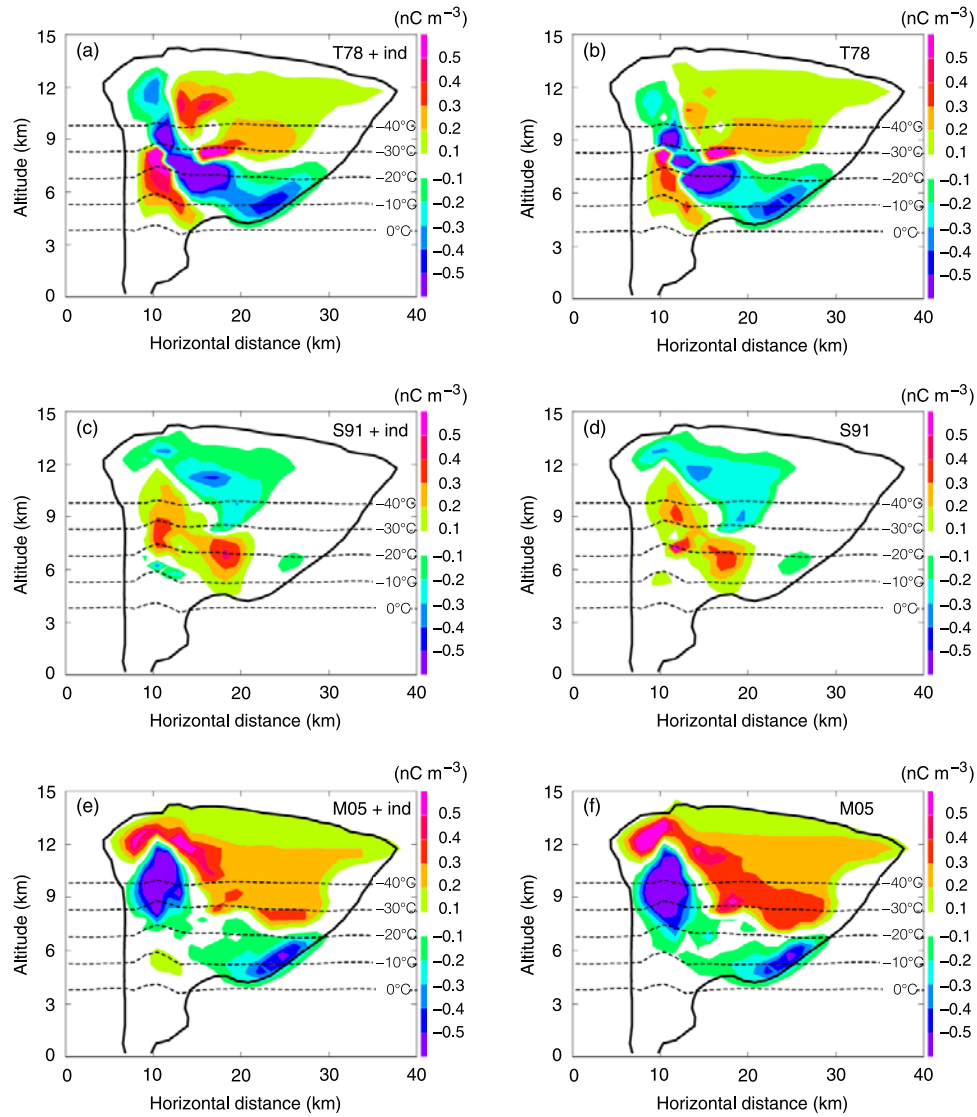


Figure 1. Vertical cross sections at 40 min of the total charge density (colored areas, in nC m^{-3}) for (a) T78, (b) T78 + ind, (c) S91, (d) S91 + ind, (e) M05, and (f) M05 + ind. T78, S91, and M05 stand for *Takahashi* [1978], *Saunders et al.* [1991], and *Mansell et al.* [2005] (modification of the original *Saunders and Peck* [1998] parameterizations). Here “ind” means that the inductive process is enabled. The 0°C , -10°C , -20°C , -30°C and -40°C isotherms are indicated. The solid line delineates the cloud boundary.

[10] For the simulations presented in the study, the positive and negative charges carried by the hydrometeors are transported by the Multidimensional Positive Definite Advection Transport Algorithm (MPDATA) scheme. The 3-D moist turbulent scheme of *Cuxart et al.* [2000] is used. To prevent the growth of undesirable numerical waves, a background fourth-order diffusion operator is applied with wave dampers placed in the top layers and in the lateral sponge zone.

[11] The 3-D simulations were performed with the following settings of the electrical scheme (see *Barthe et al.* [2005] and *Barthe and Pinty* [2007] for the meaning of these parameters): stopping electric field of the leader propagation $E_{stop} = 20 \text{ kV m}^{-1}$, grid point net charge density where branches can propagate 0.3 nC m^{-3} ,

lightning fractal dimension $\chi = 2.5$ and lightning length scale $L_\chi = 500 \text{ m}$.

3. A 3-D Multicellular Storm Case

[12] The aim of this section is to study the electrification of an idealized multicellular severe storm [*Mansell et al.*, 2002, 2005] using three noninductive charging process parameterizations. The sensitivity to the inductive process is also explored in each case.

3.1. Initialization

[13] The model domain had $40 \times 40 \times 36$ grid points with a horizontal spacing of 1 km, and a constant vertical resolution of 500 m. The time step was 2 s and the duration of the simulation was 100 min. Open lateral boundary

Table 1. Summary of Total Lightning Flash, IC, –CG, and +CG of the Sensitivity Tests^a

Charging Scheme	Total Number of Flashes	IC Number	–CG Number	+CG	IC/CG
T78	819	747	72	0	10.4
T78 + ind	905	786	119	0	6.6
S91	494	489	5	0	97.8
S91 + ind	334	329	5	0	65.8
M05	1089	1066	0	23	46.3
M05 + ind	966	909	0	57	15.9

^aT78, S91, and M05 stand for Takahashi [1978], Saunders *et al.* [1991], and Mansell *et al.* [2005] parameterizations. Adding “ind” means that the simulation is repeated with the inductive process on.

conditions were used. Convection was initiated by placing a buoyant bubble (+2 K) of radius 10 km at a distance of 10 km from the western boundary of the domain of simulation and 22.5 km from the northern boundary. The vertical profiles of temperature and moisture were taken from Weisman and Klemp [1984]. The initial wind profile of the first 5 km above the ground was taken from a half-circle hodograph with U_s , the magnitude of the wind speed, equal to 20 m s^{–1}. The wind kept its easterly direction and its magnitude above 5 km. As recommended by Weisman and Klemp [1984], taking $U_s = 20$ m s^{–1} led to a favorable dynamical environment for the development of a multicellular storm. This storm had a structure typical of continental thunderstorms in Colorado, characterized by very small droplets that render the collision-coalescence process inefficient [Dye *et al.*, 1974; Mansell *et al.*, 2005]. Consequently, supercooling was the fate of the cloud droplets in the updrafts and the formation of rain was dominated by glaciated processes. This situation was thus very favorable to strong electrical activity.

3.2. Sensitivity Tests

[14] In order to explore the sensitivity of the storm electrification scheme, three simulations were performed with different representations of the noninductive process by means of the T78, S91, and M05 parameterizations. Three additional simulations were also done with the inductive process and so are referred to as T78 + ind, S91 + ind, and M05 + ind.

[15] The vertical cross section shown in Figures 1a–1f illustrates the distribution of the total charge density after 40 min of simulation. The cross section was chosen along the axis of motion of the cells passing through the updraft core of the first cell. The lightning results are summarized in Table 1.

3.2.1. Simulations With the T78 Parameterization

[16] Figure 2a displays the vertical cross section of the noninductive and inductive separation rates linked to the graupel. The charge separation takes place in the updraft region where ice particles and supercooled droplets are colocalized as well as possible. The charging zone is 5 km wide. For each type of ice-ice collision, the largest particle, the graupel in most of the cases, gains a negative charge for temperatures between –20°C and –40°C (provided there is enough supercooled water) and a positive charge at temperatures warmer than –20°C. As the small ice crystals are located above the –20°C isotherm, collisions

involving these crystals are electrically efficient only for temperatures lower than –20°C and so ice crystals tend to charge positively. In the case of graupel-snow interactions, charge is exchanged both above and below the –20°C isotherm. The positive and negative charging rates are about ± 20 pC m^{–3} s^{–1} with values reaching 50 pC m^{–3} s^{–1} near the –25°C isotherm. As illustrated in Figure 2a, the inductive process has a sustained production of positive charges (~ 10 pC m^{–3} s^{–1}) on the graupel between 6 and 12 km altitude. This process significantly reinforces the lower positive pole of the storm (see Figures 1a and 1b) and also the electric field.

[17] An increase of the electric field is consistent with a higher flash number and more precisely with an increase of the –CG count. When T78 is used without the inductive process, the IC/CG rate is about 10 but falls below 7 when the inductive process is considered (see Table 1).

3.2.2. Simulations With the S91 Parameterization

[18] When the S91 parameterization is used, the electrical structure of the storm looks like an inverted dipole (Figure 1b). According to S91, the biggest particles always acquire a positive charge regardless of the temperature but only when the effective cloud water content (EW) is higher than 1 g m^{–3}. In contrast, for temperatures between 0°C and –20°C, and with EW lower than 0.16 g m^{–3}, the graupel particles can gain a negative charge. As a result, the multiple regimes of S91 make it extremely difficult to anticipate a charge structure of the storm. This is illustrated in Figure 2b where the noninductive separation rate of the graupel particles changes sign twice with altitude. Between the freezing level and the –12°C isotherm, the graupel particles gain a positive charge at a mean rate of 15 pC m^{–3} s^{–1}. In the temperature range of [–12, –20]°C, they tend to charge negatively at a rate of –10 pC m^{–3} s^{–1}. The charging regime reverts to the positive sign and reaches 50 pC m^{–3} s^{–1} above the –20°C isotherm as less EW is available (this regime is identified as the positive low-EW zone or PLEZ regime in the work of Mansell *et al.* [2005]). Therefore the upper negative pole in Figures 1c–1d is due to the negative charging of snow and ice crystals, while the graupel particles contribute to the lower-level positive region. Contrarily to the T78 simulation, the inductive charging of the graupel is negative because the vertical electric field is oriented downward below the main negative center of charge.

[19] A decrease of the lightning flash number is observed when S91 is used in combination with the inductive charging process. The negatively induced charges on the graupel tend to reduce the lower positive charge observed in the updraft at –10°C (see Figure 1c). Consequently with S91, the inductive process counteracts the noninductive process in the lower half of the cloud and so explains why fewer flashes are triggered when the inductive process is considered.

3.2.3. Simulations With the M05 Parameterization

[20] In this subsection, the parameterization of Saunders and Peck [1998] is adapted, partially following Mansell *et al.* [2005]. For a rime accretion rate, RAR, lower than the critical RAR, equation (20) of Mansell *et al.* [2005] is used to extend the application of the charge separation regime to RAR between 0.1 and 0.3 g m^{–2} s^{–1}. For RAR higher than the critical RAR, the original formula of Saunders and Peck

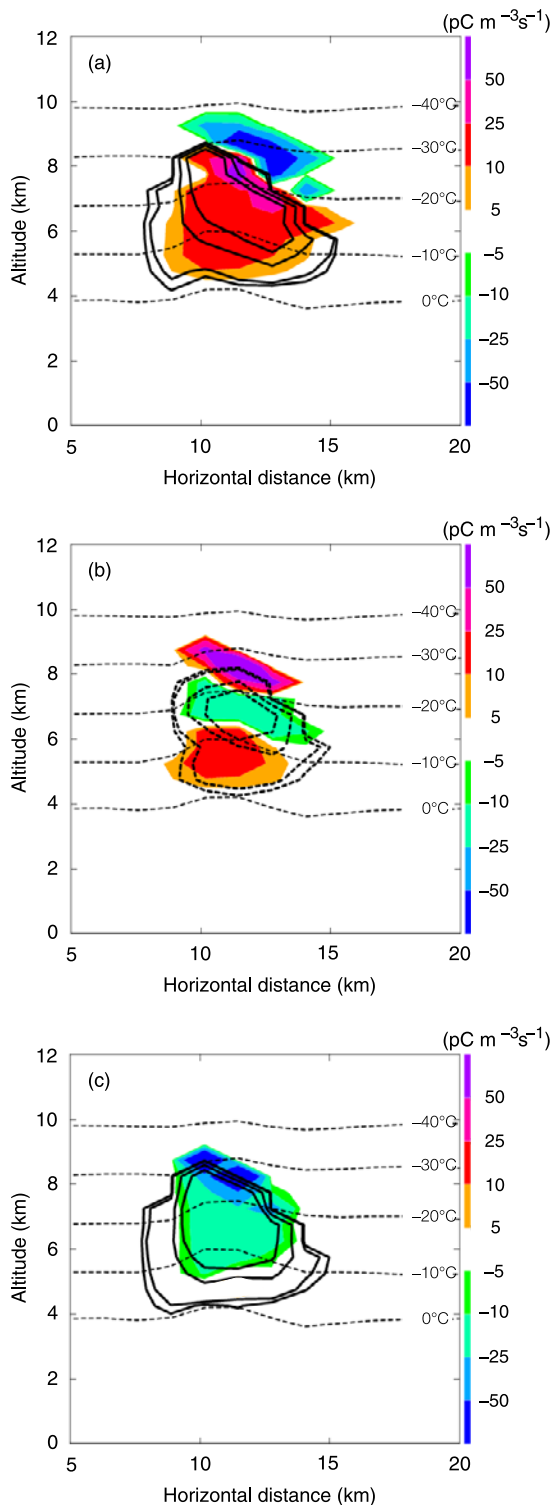


Figure 2. Vertical cross sections at 40 min of the graupel charge separation rates (in $\text{pC m}^{-3} \text{s}^{-1}$) for (a) T78, (b) S91, and (c) M05. The colored areas represent the charge separation rate by the noninductive process, while the thick black isolines represent the charging rate by the inductive process with contour intervals of ± 0.5 , ± 1 , ± 5 , and $\pm 10 \text{ pC m}^{-3} \text{s}^{-1}$. The horizontal thin dashed lines show the 0°C , -10°C , -20°C , -30°C , and -40°C isotherms. The vertical cross section is the same as in Figure 1, but the focus is on the area of interest.

[1998] is kept. Outside the temperature range of -8°C to -23°C where the original S91 is strictly valid, the charging rate is linearly decreased to zero at $0(-40)^\circ\text{C}$ from the computed value at $-8(-23)^\circ\text{C}$, as suggested by *Mansell et al.* [2005].

[21] The M05 parameterization leads to the direct dipolar structure shown in Figure 1e. This charge density configuration occurs because the charge separation regime always stays below the critical RAR curve where the graupel particles charge negatively. Between the -20°C and the -30°C isotherms, the negative charging of the graupel peaks at $-25 \text{ pC m}^{-3} \text{s}^{-1}$ (Figure 2c). As the electric field in the lower part of the cloud is directed downward, the inductive process is positive with a maximum of $10 \text{ pC m}^{-3} \text{s}^{-1}$ at 5 km altitude. So using M05 with the inductive mechanism shifts the charging process with a reduction of the lower negative charge and an increase of the upper positive charge.

[22] Table 2 shows a decrease of the total number of flashes and an increase of the proportion of +CG when the inductive process is taken into account. When a flash is triggered, the leader that propagates toward the ground is positive so only +CG are recorded.

3.2.4. Comparison With a Previous Study

[23] The simulation performed with M05 produced the largest number of IC flashes (1066) in comparison with the 747 counts with T78, and the 489 counts with S91. These values fit reasonably well those of *Mansell et al.* [2005] who obtained 988, 700 and 633 IC flashes, respectively, but for 130 min elapsed time from model start (here we selected TAK/off/50, S91/off/50, and SP98/off/50 as the best experimental conditions, which ignore the inductive process, and which are reported in Table 2 of *Mansell et al.* [2005]). So even with a simpler electrical scheme, i.e., no ions for the moment, 5 as against 12 microphysical species and a fractal branching scheme as against a full dielectric breakdown scheme, our IC lightning results confirm by the former ones of *Mansell et al.* [2005].

[24] Another point of similarity with *Mansell et al.* [2005] concerns the CG characteristics. As in the work of *Mansell et al.* [2005], +CG cannot be obtained with T78 so that our scheme triggers only -CG, but 72 as compared with 16 in the work of *Mansell et al.* [2005]. +CG exclusively are found (23 counts) with M05 while *Mansell et al.* [2005] obtained 5 +CG and 7 -CG in this case, and six flashes of each polarity with S91/off/50, to be compared with 5 -CG in our corresponding case. This difference is attributable to the more complex charge structure in *Mansell et al.*'s simulations where the formation of screening layers offers the existence of positive and negative CGs along the course of the simulation. Furthermore, the lower spatial resolution of this study (1 km against 500 m) is probably less favorable to a high supercooled water content, which is indeed critical for switching between the charging regimes (especially with the M05 case for which crossing the critical RAR boundary is difficult).

[25] Concerning the importance of the inductive process, *Mansell et al.* [2005] reported that their "strong" version of the charging process nearly doubled the IC rate in all cases while the "moderate" version, the same as ours, weakly reduced the IC number of flashes. Our results in Table 1 do not suggest exactly the same conclusion. The inductive

Table 2. Lightning Flash Characteristics and Cloud Electrical Structure for the T78, S91, and M05 Noninductive Process Parameterizations Applied to Three Convective Events^a

	Charging Scheme	Total Flash Number	−CG Number	+CG Number	Cloud Electrical Structure
Squall line (mature stage)	T78	641	38	0	Inverted dipole
(Wmax = 16 m s ^{−1})	S91	384	0	0	Direct dipole
Duration 1 h	M05	0	0	0	Direct dipole
Supercell storm	T78	604	2	0	Inverted dipole
(Wmax = 19 m s ^{−1})	S91	122	0	0	Inverted/direct dipole
Total duration 1 h 20 min	M05	124	0	0	Direct dipole
Multicell storm	T78	905	119	0	Tripole
(Wmax = 57 m s ^{−1})	S91	334	5	0	Inverted dipole
Total duration 1 h 40 min	M05	966	0	57	Direct dipole/tripole

^aWmax is the recorded maximum updraft velocity. The simulation duration includes the cold start growth of the cellular convection (the rise of a buoyant bubble).

process may have a favorable (T78) or an adverse (S91 and M05) effect depending on the polarity of the multicell storm and on the orientation of the electric field. The situation is less complex for the CG flashes as their proportion (the ratio CG/(IC + CG)) increases when the inductive process is considered. The enhanced sensitivity of the CG number to this secondary electrification process is consistent since the inductive process operates in the lower part of the cloud where graupel particles and supercooled droplets are most likely to be present.

3.2.5. Comparison With Observations

[26] Three-dimensional lightning mapping systems based on the detection of VHF sources from lightning have permitted to investigate the cloud electrical structure. Indeed, those observations reflect the basic charge structure of electrified storms [Rison *et al.*, 1999]. Krehbiel *et al.* [2000] have shown the evidence for three main charge levels in the storm. The main negative charge is located in the middle level at 5–6 km msl and the upper level would correspond to the upper positive charge [Shao and Krehbiel, 1996]. This electrical cloud structure is supported by a number of observational studies [Dye *et al.*, 1986; Thomas *et al.*, 2001; Rison *et al.*, 1999]. A lower positive charge playing a role in CG flashes is also located at 3–5 km msl near the 0°C isotherm. Using S91 to simulate the non-inductive charging in the multicell leads to a charge structure opposed to the commonly observed one. T78 and M05 give an electrical structure in better agreement with observations than S91. The main negative charge is located between 6 and 8 km altitude. The upper positive charge extends above 9 km. A lower positive charge region also appears in the T78 simulation. However and even if T78 results for charge structure seem to better match with observations, it is not really possible to conclude about the suitability of this parameterization. Indeed, other charge structures has been observed as inverted dipole [Rust and MacGorman, 2002; Rust *et al.*, 2005] or more complex structures [Stolzenburg *et al.*, 1998b].

4. 2-D Simulation of a Tropical Squall Line

[27] Typically, a two-dimensional mature squall line evolves slowly in its moving frame of reference. This makes this type of organized mesoscale convective system a good candidate for the study of the electric charge budgets and lightning flash rates in well-depicted convective and strati-

form regions with heavy and light precipitation, respectively. The aim of the study was to investigate the dominant electrical processes that take place in each region. It is then instructive to explain and to relate the different electrical states of the squall line to the dynamical and microphysical contrasts of this system.

4.1. Storm Initiation

[28] The tropical squall line chosen for the simulation occurred on 23 June 1981 during the COPT81 experiment in the north of Ivory Coast. The simulation and the model initialization followed Caniaux *et al.* [1994]. The sounding (not shown here) showed a strong shear of 0.006 s^{−1} approximately in the first 3000 m above ground level. The horizontal domain comprised 320 grid points with a resolution of 1.25 km. The vertical grid contained 46 unevenly spaced levels up to 22 km with a grid length stretching from 70 m at the ground to 700 m at the top of the domain. The time step of the integration was 5 s. Convection was initiated by a cold pool perturbing the initially homogeneous atmosphere. A constant 0.01 K s^{−1} cooling rate was applied for 10 min to a region 12 km long and in the first 4 km of atmosphere above the flat ground. Open boundary conditions were used in the x-direction. A galilean transformation of −13 m s^{−1} was applied to keep the system in the simulation domain. The duration of the simulation was 8 h, the time needed by the squall line to reach a mature stage and stay in it. The parameterization of Takahashi [1978] was considered for the noninductive electrical process. The inductive charging process was also taken into account. The lightning flash scaling parameters were adapted to a 2-D simulation with $\chi = 1.8$ and $L\chi = 1000$ m.

[29] Figure 3 represents the vertical velocity averaged over the last hour of the simulation. The system moves from the right to the left, and therefore the youngest convective cells are on the left flank of the convective system. Two different regions can be distinguished in the squall line. The 40-km-wide convective region is characterized by a maximum vertical velocity of a few meters per second. This region produces the largest portion of the total precipitation of the system. The stratiform region with much moderate precipitation stretches over more than 200 km at the rear of the system. These two major zones are separated by a transition zone with light precipitation. As shown in Figure 3, the stratiform region is characterized by an upward

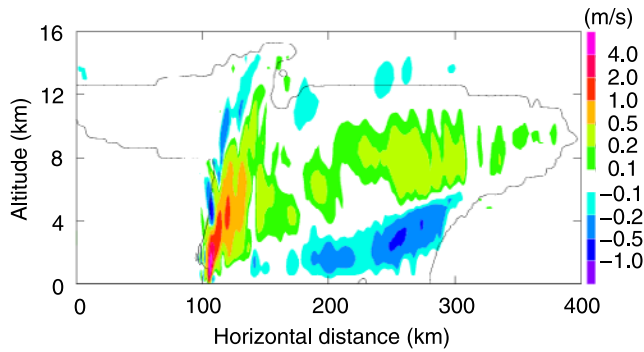


Figure 3. Vertical cross section of the 1-h averaged vertical velocity (colored areas, in m s^{-1}) during the mature stage of the squall line. The solid line depicts the cloud boundary.

air motion overlying subsident air due to rain evaporation in the low levels, i.e., between the ground and 4 km altitude.

4.2. Mean Microphysical Profiles in the Convective and Stratiform Regions

[30] The convective zone corresponds to the cloudy region where the precipitation rate exceeds 5 mm h^{-1} while the stratiform region is associated with atmospheric columns having surface precipitation rates lower than 5 mm h^{-1} . The budgets are obtained after performing a 1-h horizontal average over each zone to obtain vertical budget profiles.

[31] The mean profile of the mixing ratio of each hydrometeor is shown in Figure 4. In the convective region, the pristine ice crystals are found between 5 and 12 km with a maximum of 0.21 g kg^{-1} at 8 km. The snow maximum mixing ratio is about 0.37 g kg^{-1} at 7.5 km of altitude. The graupel mixing ratio reaches 1.2 g kg^{-1} at 5 km altitude. On melting, graupel transforms into raindrops with a peak mixing ratio of 0.7 g kg^{-1} at ground level. The cloud droplets are mostly present in the lower levels where they help to increase the raindrop mixing ratio by autoconversion. They are also present in significant amounts ($\sim 0.02 \text{ g kg}^{-1}$) in the

glaciated part of the convective cells in the 5–10 km range of altitude.

[32] All the categories of hydrometeors are present in the stratiform part of the squall line but with a reduced mixing ratio compared to that of the convective region. A noticeable difference is that the snow/aggregate category now dominates with a peak value of 0.2 g kg^{-1} at 7 km. Owing to their low individual masses, snow and ice crystals can be transported rearward from the top of the convective region to the adjacent stratiform region. A similar detrainment is not possible for the graupel because these particles have an appreciable size and density. So they fall faster and, furthermore, they are mostly present in the lower levels. As a result, the graupel, with a peak value of 0.18 at 5 km, must be produced locally by the riming of snow as little supercooled water is present up to 10 km altitude. The presence of a small fraction of supercooled water in the rear part of the system is consistent with the mesoscale updraft [Leary and Houze, 1979; Zrnić et al., 1993; Braun and Houze, 1994; Caniaux et al., 1994]. These authors show that the mesoscale updraft in the stratiform region of a squall line can be intense enough to sustain a sufficient amount of supercooled water to produce graupel particles.

4.3. Mean Profiles and Budget of Electric Charges

4.3.1. Convective Region

[33] Figures 5a and 5c show the mean vertical profiles of the individual and total electric charge densities of the convective region. The charge density attached to the water vapor field changes its polarity: it is positive below 4.5 km and negative above this altitude. As explained by Barthe and Pinty [2007], ions are not explicitly treated in Méso-NH for the moment. Therefore and unlike in the work of Altaratz et al. [2005], the conservation of the total charge density makes it necessary to take into account the electric charges released during the evaporation of the raindrops and the sublimation of the ice particles. For convenience, these net charges are symbolically “attributed” to the water vapor and so they move with the air flow. The charge density of the cloud droplets is very low and so it is absent from

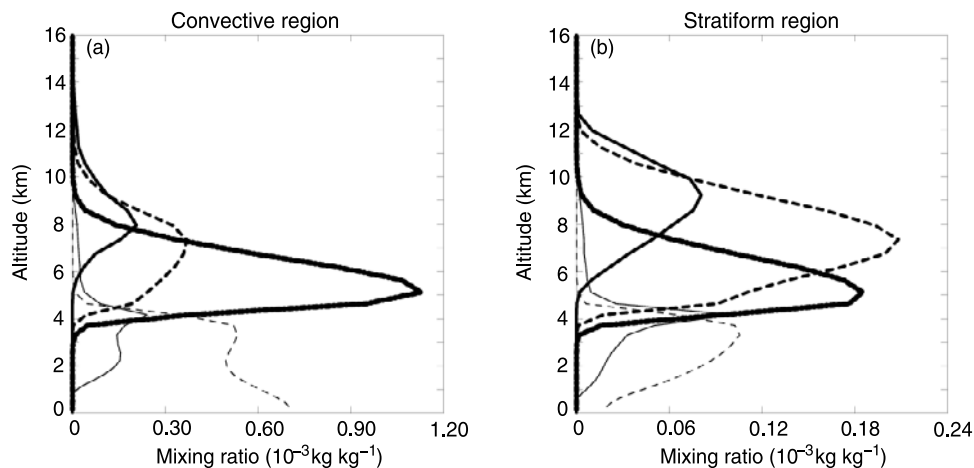


Figure 4. Hydrometeor mean mixing ratios for the (a) convective and (b) stratiform regions of the squall line. The profiles are drawn for the cloud droplets (thin solid line), raindrops (thin dashed line), pristine ice (solid line), snow (thick dashed line), and graupel (thick solid line).

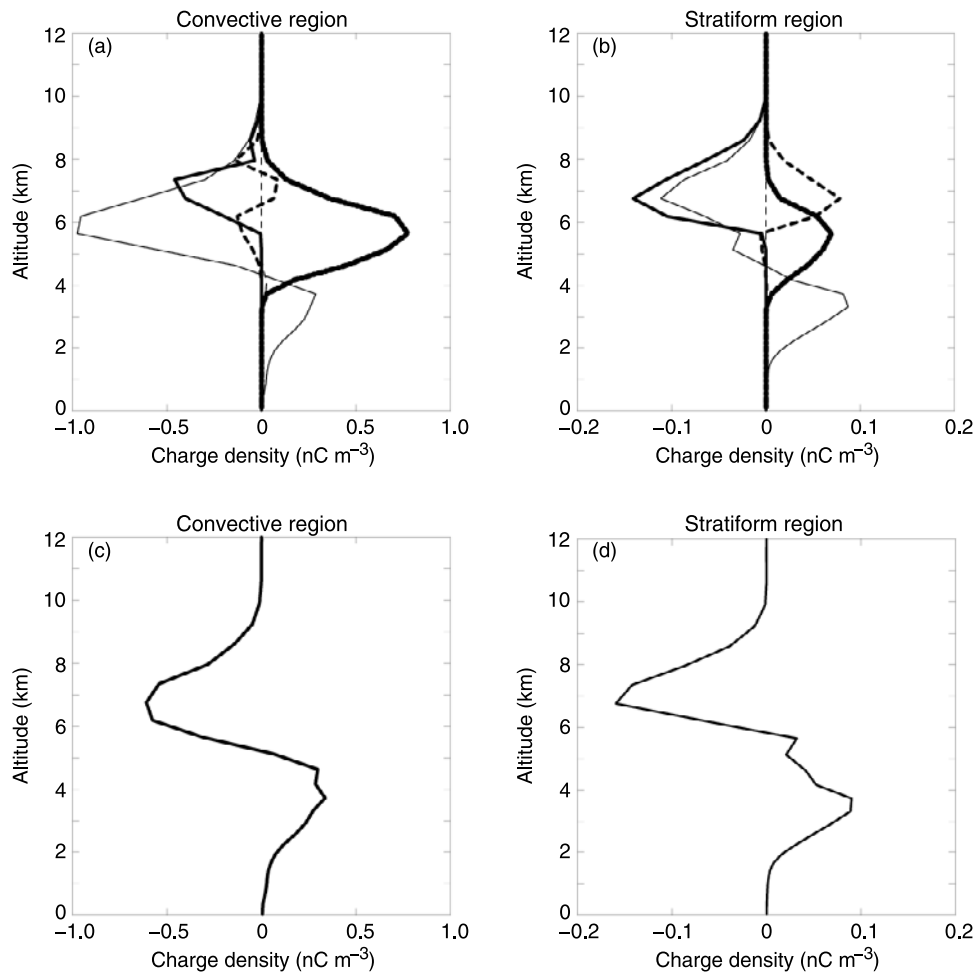


Figure 5. Profiles of (top) individual and (bottom) total mean charge densities in (right) the convective region and (left) the stratiform region of the squall line. The profiles correspond to the charge carried by water vapor (thin solid line), raindrops (thin dashed line), pristine ice (solid line), snow (thick dashed line), and graupel (thick solid line).

Figure 5. The raindrops are weakly positively charged between the ground and 4.5 km. The pristine ice crystals have a negative polarity. Their charge density becomes significant between 5.5 km and 9 km altitude. The snow charge density oscillates with altitude. It is negative between 4 km and 6.5 km, positive in the altitude range of 6.5–7.5 km, and negative again up to 9 km. In the convective region, the majority of the charges come from the graupel, with a peak charge density of $+0.75 \text{ nC m}^{-3}$ at 5.5 km, and from the water vapor, which approximates a net effect of small ions. The total charge density (Figure 5c) looks like an inverted dipole with negative charges around 7 km above positive charges centered at 4.5 km.

[34] The different terms of the electrical budget of the ice crystals and of the graupel in the convective region are now analyzed in Figures 6a and 6c, respectively. As expected, the noninductive charging process is dominant for each category of ice particle with rates varying between -2.3 and $+1.5 \text{ pC m}^{-3} \text{ s}^{-1}$ for the ice crystals and with a single peak at $+2.0 \text{ pC m}^{-3} \text{ s}^{-1}$ for the graupel. The noninductive snow charging rate (not shown here) is symmetrical to the sum of the charging rate profiles of the small ice crystals and

graupel. The positive and negative charging rates of the small ice crystals correspond to the ice-snow and ice-graupel noninductive charging rates, respectively. The graupel particles acquire their positive charge mostly by interacting with snow (see Figure 4a). It is questionable why ice crystals are negatively charged whatever the altitude (Figure 5a), whereas a strong noninductive mechanism should create a positive pole at the top of the convective cells (Figure 6a). In reality, the simulation shows the formation of short-lived narrow pockets of positively charged ice crystals which migrate toward the stratiform region of the squall line where they dilute with negatively charged crystals. The positive charging of these crystals comes from the region of polarity reversal of the T78 diagram because enough supercooled water is available at temperatures lower than -25°C . It is the upward transport of negative crystals which contributes the most to the accumulation of negative crystals above 7 km. The other processes (microphysical transfer processes and neutralization) only weakly counteract the positive charging of the ice crystals at altitude.

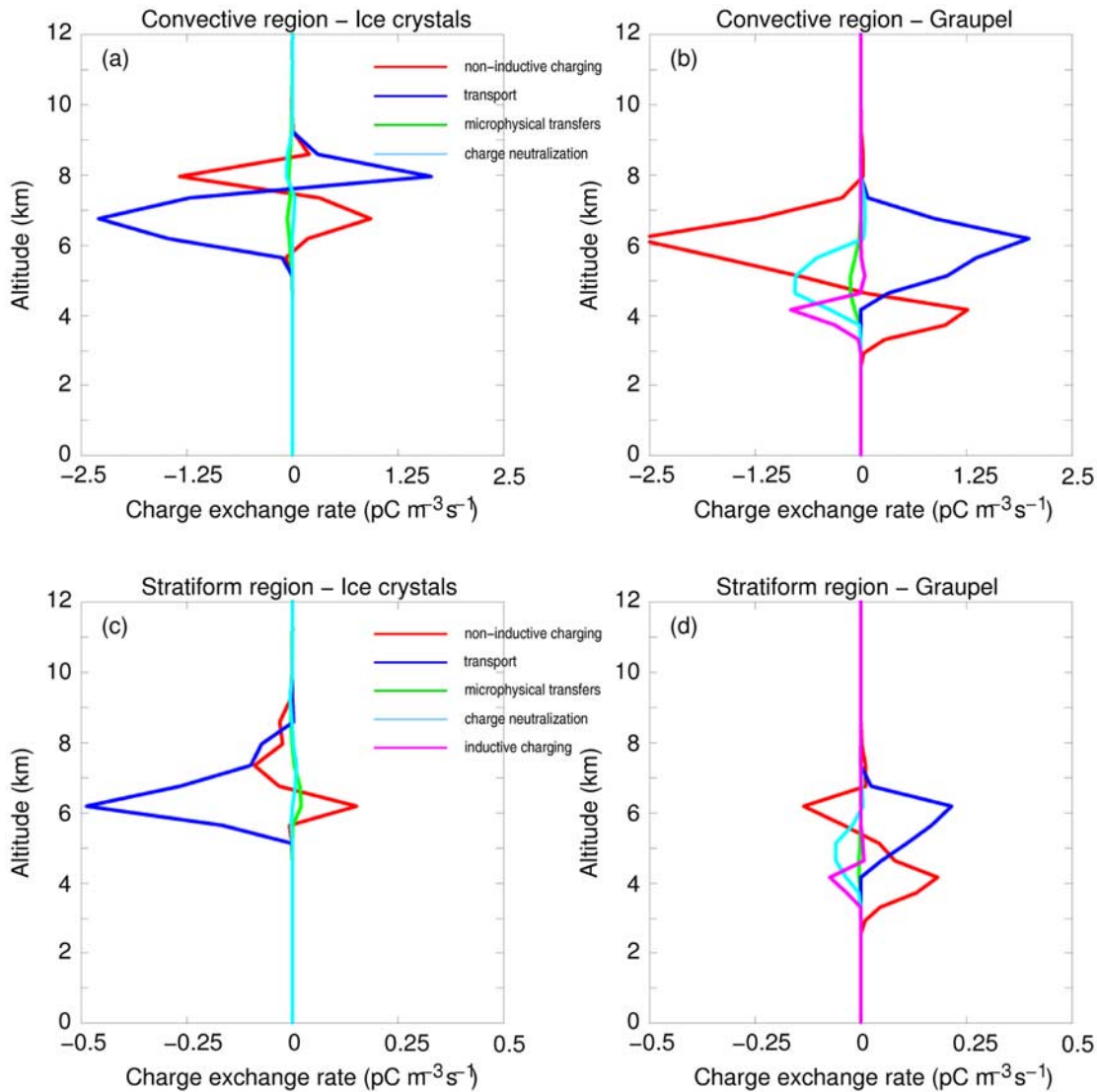


Figure 6. Budgets of the electrical charge profiles of (top) the ice crystals and (bottom) the graupel in (right) the convective region and (left) the stratiform region.

[35] Concerning the budget of the graupel particles displayed in Figure 6c, the noninductive charging rate is balanced by the sedimentation of these hydrometeors (a downward flux of positive graupel). The inductive charging rate is negative as expected for an upward pointing electric field. This process has a nonnegligible contribution in the low levels, $-1.0 \text{ pC m}^{-3} \text{ s}^{-1}$ at 4 km altitude, where the noninductive charging process is not possible. The neutralization of the positively charged graupel by the lightning flashes is equivalent to a net addition of negative charges ($-1.0 \text{ pC m}^{-3} \text{ s}^{-1}$ at 5 km altitude). In comparison, microphysical transfer rates are very slow on average, but they are indeed necessary to transfer charges to the droplets when the inductive process is not considered.

4.3.2. Stratiform Region

[36] The detailed and net charge density profiles are shown in Figures 5b and 5c, respectively. On average, the charge densities are five times lower in the stratiform region than in the convective area. Note that a similar proportion

holds for the mixing ratios (see Figures 4a–4b). The less prominent role of graupel for the microphysics, and consequently for the electrical charging of the squall line, is also the distinguishing feature between the convective and the stratiform areas. The inverted dipole structure is preserved.

[37] Figures 6b and 6d confirm that electric charges can be produced locally in the stratiform part of the squall line. A significant amount of liquid water is available between isotherms 0°C and -10°C . In Takahashi's diagram, this range of temperature corresponds to a positive charging of the graupel and snow particles. The maximum charging rate tendencies of the graupel particles ($\sim 0.25 \text{ pC m}^{-3} \text{ s}^{-1}$) are one tenth of those in the convective region. As a result, the ice crystals are always negatively charged at altitude, leaving an inverted dipole structure (Figure 5d). Figure 5b shows that a marked contribution to the positive pole (peak at 3 km height) comes from the evaporation of rain, which liberates the positive charges that are traced by the “water vapor charge” signal.

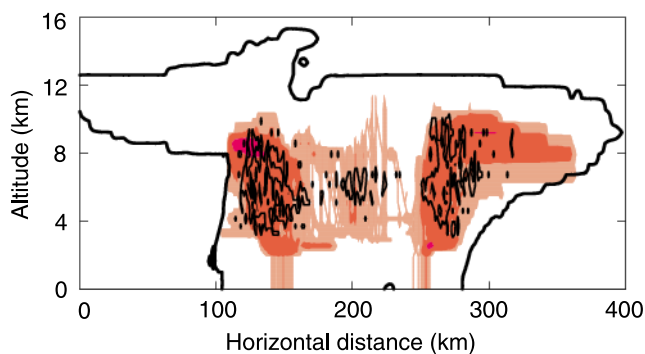


Figure 7. Vertical cross section of the 1-h lightning flash triggering altitude (in black) and lightning flash density (no units, in color with increasing density from brown to red). Two locations of CG flashes are easily detectable. The black solid line is the cloud boundary.

[38] The imbalance on the small ice crystal electric budgets, a negative trend which shows up between 5 and 7 km in Figures 6a–6b, is due to an extra charge transfer term (not plotted) between the ice crystals and the water vapor. This correction is necessary to eliminate an unrealistically large charge density on residual amounts of ice crystals. The charge conservation requirement leads us to restore these charges on the “water vapor” term.

[39] Charge advection is not of significant importance in the simulated squall line. Indeed, the model does not reproduce the observed upper layer of charge. Thus only a few negatively charged ice crystals are advected from the convective to the stratiform region. It leads to only a light enhancement of the upper negative charge of the stratiform region. The probable advection of the two upper layer of charge in the *Stolzenburg et al.* [1998a] diagram is not reproduced.

4.4. Discussion

[40] The budgets calculated with Méso-NH on the 2-D squall line display the in situ charging of the stratiform region by a noninductive mechanism. This is consistent with observations revealing the coexistence of snow, graupel, and supercooled water in the stratiform region by *Zrnić et al.* [1993]. They show that the mesoscale updraft is intense enough to sustain a sufficient amount of supercooled water and to produce graupel particles. From electric field soundings and Doppler radar analyses, *Schuur et al.* [1991] suggest that the charge in the stratiform region may have been advected from the convective region. They underline that in situ charging can also be active. From results of 2-D simulations of a tropical mesoscale convective system, *Schuur and Rutledge* [2000] also conclude in favor of local charging in the stratiform region to explain the observed charge densities.

[41] Analyzing 15 electric field soundings inside and outside updrafts, *Stolzenburg et al.* [1998a] have shown that the electrical structure of a squall line is more stratified than the dipole or tripole picture. Their results reveal that four layers of charge are present in the convective region and six outside the updraft. *Stolzenburg et al.* [1998c] deduce that the upper negative layer comes from the screening effect, while the noninductive mechanism can

account for the three lowest layers. Outside the updraft, the noninductive process cannot explain the complex electrical structure by itself, even without the screening layer. Other processes have to be considered, like transport or other charging processes. In Méso-NH, the ions are not treated explicitly; therefore the upper screening layer cannot be obtained. Concerning the lower tripole in the convective region, the model fails to reproduce it. The updraft is not intense enough for this tropical squall line case to loft supercooled water to high levels, so the majority of the ice crystals cannot become positively charged. Another explanation can be sought in the parameterization of the charge separation process. This hypothesis is explored in the last section of the study. However, the locations of the lower positive pole and of the negative region are consistent with observations by *Carey et al.* [2005]. They found a tripole structure in the convective region of a mesoscale convective system with the positive charge centered at about 4.5 km and 9.5 km and the negative charge located around 7 km. The Méso-NH results are consistent with the two observed lower poles as the positive and negative regions are centered at 4 km and 7 km altitude, respectively.

[42] The positive charge in the stratiform part located around 4 km (0°C isotherm) is also in agreement with the numerous observations in mesoscale convective systems [*Stolzenburg et al.*, 1994; *Marshall et al.*, 2001]. However, those studies reported more complex charge structures. This is a drawback from the model. A possible explanation is the failure of the model to produce charge in altitude and especially in the convective part where charge could be advected to the stratiform area. Concerning the COP81 squall line, *Chauzy et al.* [1985] deduced from their electric field soundings that the more often observed electrical structure was a direct dipole (positive charge above negative charge). They also observed positive charge screening layer at the base of the cloud and/or negative charge screening layer at the top of the cloud. However, these regions of charge were much less intense than the two main charge regions that made them conclude in favor of a direct dipole.

4.5. Lightning Flash Activity and Conclusion

[43] Figure 7 displays the locations where lightning flashes are triggered and also the areas where the lightning flashes propagate. It can be seen that the lightning flashes are preferentially triggered in the convective region, but a substantial fraction of them are found in the stratiform plume of the squall line. Most of the flashes originate in the levels between 5 and 6 km. This altitude corresponds to the -10°C isotherm which is located midway between the inverted dipoles of Figures 5c and 5d. The lightning flashes have a large horizontal extension (up to 100 km) in the stratiform region.

[44] Negative CG flashes are found in both the convective and the stratiform regions (see the two colored bars connected to the ground in Figure 7). During the last hour of simulation, a total of 718 flashes is triggered including 75 –CG, but no +CG. *Parker and Johnson* [2001] analyzed different mesoscale convective systems and concluded that –CG are triggered in the convective part, whereas +CG are possible in the stratiform part. As noted by *Mansell et al.* [2002, 2005], +CG flashes require a lower negative charge region to be triggered, while –CG flashes need a lower

positive charge. In Takahashi's diagram, the largest particle gains a positive charge at temperatures warmer than -10°C whatever the liquid water content is. This explains why the lower pole of the cloud electrical structure is always positive when T78 is used. Therefore no +CG can be initiated when the T78 parameterization is used. However, +CG are commonly observed in mesoscale convective systems as reported by Lang *et al.* [2004]; Zajac and Rutledge [2001]; Rutledge and MacGorman [1988]; Rutledge *et al.* [1990]. Stolzenburg *et al.* [1994] shows that the +CG may be associated with very tall storms that produce hail. Lang *et al.* [2004] showed that +CGs in the stratiform region originate both from the convective line and the stratiform region. Whether in the convective or in the stratiform region, Meso-NH fails in reproducing this typical feature of mesoscale convective systems.

[45] In conclusion, the model simulates an electric charge structure of a 2-D tropical squall line simpler than usually observed. However, the model does not reproduce the +CG flashes usually observed in the stratiform part of mesoscale convective systems. While this type of convective system has a contrasted dynamical and precipitation regime, the differences between the electrical properties of the convective and the stratiform parts are qualitatively not very marked. As expected fewer electric charge are locally separated in the stratiform area. However, the separated charge is high enough to allow flash triggering in the stratiform part of the squall line. Even if the T78 scheme seems more adapted for the multicellular storm, it is difficult to conclude about the suitability of the T78 scheme to reproduce the electric charge structure of a squall line as the model fails in reproducing +CG that are characteristics of the stratiform part.

5. Analysis of the Electrification of Different Convective Events

[46] The electrification of three convective systems, a squall line, a multicellular storm, and a supercellular storm, has been simulated. The squall line and the multicell cases are described in this paper, while the supercell case was investigated in the work of Barthe *et al.* [2005] and in the work of Barthe and Pinty [2007]. In each case, a series of simulations were performed that differed from the parameterization of the noninductive process (the inductive charging was activated). As in the work of Helsdon *et al.* [2001] and Altaratz *et al.* [2005], the T78 and S91 parameterizations were explored. In addition, the reworked M05 parameterization, deduced from Saunders and Peck [1998] but adapted by Mansell *et al.* [2005] as described above, was also tested. The results are summarized in Table 2. The electrical structure of the squall line is examined during the mature, quasi-stationary state of the mesoscale system.

5.1. T78 Results

[47] The charge structure obtained with the parameterization of Takahashi [1978] is an inverted dipole in the squall line and the supercellular storm cases while the multicellular storm gives a tripole. The reason lies in the too weak updrafts of the squall line and of the supercell, which cannot sustain a significant amount of supercooled water at altitude to produce a positive charge layer above the

-20°C isotherm. In the squall line and supercell simulations, the noninductive charge separation mechanism exists below the -25°C isotherm, while in the multicellular case, the electrification process is efficient up to the -35°C isotherm (Figure 2a). When the liquid water content is high enough at -20°C , the pristine ice crystals acquire a positive charge and contribute to the positive polarity of the anvil. In the squall line and in the supercell cases, the updraft does not exceed 20 m s^{-1} , and the charging region is confined between the freezing level and the -20°C isotherm. As a result, the graupel particles become massively positive. Only -CG can be triggered in the three convective events, in agreement with the study by Mansell *et al.* [2005].

5.2. S91 Results

[48] The implementation of the S91 parameterization in the model produces the fewest IC and CG flashes. During the mature stage of the squall line, the charge structure looks like a direct dipole in accordance with the sparse observations reported by Chauzy *et al.* [1985]. The supercellular storm starts with an inverted dipole that switches into a direct one 10 min later [Barthe and Pinty, 2007]. For the two convective cases, the charging occurs below the -20°C isotherm. The graupel first charges positively between 0°C and -10°C and negatively above. A few minutes later, the negative charging of the graupel is reinforced at altitude because ice crystals and supercooled water are transported higher by the updraft. Once the inverted dipole has been created, a direct dipole forms due to a shallow negative layer at cloud base. In contrast, the electrical structure of the multicellular case is an inverted dipole throughout the simulation. Again, the main difference with the two other cases is the high efficiency of the noninductive charging up to the -30°C isotherm (Figure 2b). The positive charging of the graupel in the upper region of the cloud corresponds to a negative anvil. Only 5 -CG are triggered during the multicell lifetime, but none in the two other cases with S91. In comparison, fewer CG are triggered with S91 than with T78 because the boundary between the two regions of opposite polarity is located at a higher altitude.

5.3. M05 Results

[49] All the simulated cases lead to a direct dipole or tripole. The reason is that the critical RAR seems too high to allow positive charging of the graupel at low altitude (RAR never exceeds $1\text{ g m}^{-2}\text{ s}^{-1}$ in the squall line and supercell cases). A high variability is observed for the number of lightning flashes: 0 for the squall line, 124 for the supercell and 966 for the multicell. As shown in Table 2, M05 is the only parameterization that produces positive CG flashes. No IC flash is triggered in the squall line case because of the too weak electrification rate at this stage of the storm.

5.4. Summary

[50] Many studies have investigated the role of the noninductive process in the electrification of thunderstorms. As found in other case studies [Helsdon *et al.*, 2001; Mansell *et al.*, 2005; Altaratz *et al.*, 2005], using S91 in our squall line and supercell cases led to an inverted dipole followed by an inversion of polarity 10 min later. M05 was the only scheme that was able to produce +CG flashes in the three simulated cases. With T78, no +CG was triggered.

Concerning S91, the complexity of the charging rate diagram made it difficult to conclude about the effectiveness of the parameterization to produce +CG. Only 5 CG were obtained for the three simulations but, as the lower charge region was always positive, it precluded the formation of +CG. This analysis is consistent with the conclusions of *Mansell et al.* [2005] who indicate that +CG discharges need a lower negative charge region. Our results confirm that the inductive process becomes important once electrification is initiated by the noninductive process. The inductive process favors the production of CG flashes [*Mansell et al.*, 2005].

[51] This study shows that the electrical behavior of the storm depends not only on the noninductive parameterization but also on the storm type and storm intensity. The reason for this is that high vertical wind speeds fuel more supercooled water in the storms and the amount of supercooled water is a key parameter of the noninductive charging regimes (see the diagrams plotted by *Mansell et al.* [2005]). So most of the present modeling uncertainty comes from the delineation and the thresholds between the different charging regimes of T78, S91, and M05. For example, the electrification of the same multicell storm shows that T78 and M05 lead to opposite results in the charge structure and CG polarity.

[52] As seen in section 3, the T78 parameterization suits better to the observations of a classic tripole [*Williams*, 1989]. However, when applied to the 2-D squall line, T78 fails in reproducing the direct dipole described by *Chauzy et al.* [1985] or the more complex structure of *Stolzenburg et al.* [1998b]. Moreover, none of the noninductive parameterizations can reproduce the +CG production in this squall line. Table 2 shows a wide variety of electrical structure and CG/(IC + CG) ratios. All those electrical structures have been observed in nature from the simple direct [*Chauzy et al.*, 1985] or inverted dipole [*Rust and MacGorman*, 2002; *Rust et al.*, 2005] to tripole [*Williams*, 1989] or an even more complex structure [*Stolzenburg et al.*, 1998b]. A wide variety of CG/(IC + CG) ratio can also be found in the literature (*Livingston and Krider* [1978], *MacGorman and Burgess* [1994], and *Carey and Rutledge* [1996], among others) making difficult to conclude about which noninductive formulation suits best for cloud electrification. Therefore the next step will be the simulation of a well-documented real case in order to directly compare model results to observations dedicated to this storm.

[53] Besides the many gaps in our understanding of the cloud electrification process, some uncertainties and improvements can be pointed out in the present model. First, simulations have shown the importance of the liquid water content in determining the charging regime. However, supercooled water is a residual which is difficult to equilibrate in any microphysical scheme [*Lascaux et al.*, 2006]. Second, ions are not explicitly treated in the model. Yet they are necessary to produce screening layers at the top of the cloud, and to better represent the physics of the neutralization process. Third, hail is not taken into account in the electrical scheme of Méso-NH although it is explicitly considered as a full category of hydrometeor in an updated version of the microphysical scheme. The role of hail in electrified severe storms and the link with +CG was recently

highlighted by *Stolzenburg et al.* [1994]; *MacGorman and Burgess* [1994]; *Wiens et al.* [2005].

6. Conclusion

[54] An electrical scheme has been used to study the life cycle of the electric charges and the bulk characteristics of lightning flashes in a three-dimensional mesoscale model [*Barthe et al.*, 2005]. The study was performed for different idealized convective conditions in order to catch some persistent features of the electrical scheme. First, the case of a highly convective multicell storm has been examined for different parameterizations of the noninductive mechanism [*Mansell et al.*, 2005]. Even under the same dynamical and microphysical conditions, the electrical polarity and the lightning characteristics are strongly dependent on the noninductive parameterizations tested: T78, S91, and M05. Furthermore, model results show a sensitivity to the inductive charging which increases or decreases the number of flashes but always lowers the IC/CG ratio.

[55] The simulation of an African mature tropical squall line offered the opportunity to study the microphysics and the electrical budget of the convective and stratiform parts. A salient result is that the amount of supercooled water is high enough in the stratiform region to produce graupel and hence to separate electric charges by a noninductive process. This is consistent with the conclusion of *Schuur and Rutledge* [2000]. The resulting charge structure obtained with the parameterization of *Takahashi* [1978] is an inverted dipole which is not in agreement with the observations of *Stolzenburg et al.* [1998a] in the US. The difference between model results and observations (vertical profiles of charge structures retrieved from electric field soundings) is partially attributable to the small ions that are not physically considered in the model or to the weakness of the updrafts which cannot create a positive pole with the pristine ice crystals in the upper levels. IC and CG flashes are triggered in both part of the squall line.

[56] IC and CG flashes are triggered in both part of the squall line, but no +CG flashes are triggered whatever noninductive parameterization is used. The M05 parameterization is the only one able to produce +CG, but it does not electrify the squall line enough to trigger flashes.

[57] Finally, the simulation of several storms, each carried out with three different noninductive parameterizations, shows the occurrence of inverted/direct dipole and tripole structures while \pm CG can be obtained accordingly. This result is encouraging because it demonstrates that the model clearly responds to the various charge separation schemes. The T78 and M05 schemes have dominant opposite effects: the graupel charges positively with the former and negatively with the latter (each configuration producing CG flashes of opposite polarity).

[58] The next step is to simulate well-documented cases like those recently observed during the STEPS field program in 2000 [*Lang et al.*, 2004]. For instance, *Rust and MacGorman* [2002] and *Rust et al.* [2005] inferred from electric field soundings and lightning mapping data that inverted-polarity structures and +CG were frequently identified during STEPS. In their detailed study of a severe hailstorm STEPS case, *Wiens et al.* [2005] conclude that the presence of a lower negative charge region seems to be a

requirement for +CG. This result is consistent with *Mansell et al.* [2002, 2005] and the present study, for which +CG (−CG) flashes require a lower negative (positive) charge region for initiation. Therefore we can conclude that catching the natural variability of the electrical structure of the storms depends very much on the validity of the noninductive charge separation scheme. So far the models provide the right kinematical and microphysical (ice particles and supercooled water) conditions.

[59] **Acknowledgments.** Computational support for this research was provided by IDRIS (Institut de Développement et de Recherche en Informatique) in Palaiseau under project 2005-0569. Thanks are due to E. Mansell (CIMMS, University of Oklahoma, Oklahoma, USA) for providing us with the multicell case sounding. The authors would like to thank Pr. Serge Chauzy (LA) for helpful discussions concerning the electric charge structure of the COPT81 squall line.

References

- Altartaz, O., T. Reisin, and Z. Levin (2005), Simulation of the electrification of winter thunderclouds using the three-dimensional Regional Atmospheric Modeling System (RAMS) model: Single cloud simulations, *J. Geophys. Res.*, *110*, D20205, doi:10.1029/2004JD005616.
- Barthe, C., and J.-P. Pinty (2007), Simulation of a supercellular storm using a three-dimensional mesoscale model with an explicit lightning flash scheme, *J. Geophys. Res.*, *112*, D06210, doi:10.1029/2006JD007484.
- Barthe, C., G. Molinié, and J.-P. Pinty (2005), Description and first results of an explicit electrical scheme in a 3D cloud resolving model, *Atmos. Res.*, *76*, 95–113.
- Braun, S. A., and R. A. Houze (1994), The transition zone and secondary maximum of radar reflectivity behind a midlatitude squall line: results retrieved from Doppler radar data, *J. Atmos. Sci.*, *51*, 2733–2755.
- Caniaux, G., J.-L. Redelsperger, and J.-P. Lafore (1994), A numerical study of the stratiform region of a fast-moving squall line. Part I: General description and water and heat budgets, *J. Atmos. Sci.*, *51*, 2046–2074.
- Carey, L. D., and S. A. Rutledge (1996), A multiparameter radar case study of th microphysical and kinematical evolution of a lightning producing storm, *J. Meteorol. Atmos. Phys.*, *59*, 33–64.
- Carey, L. D., W. A. Petersen, and S. A. Rutledge (2003), Evolution of cloud-to-ground lightning and storm structure in the Spencer, South Dakota, tornadic supercell of 30 May 1998, *Mon. Weather Rev.*, *131*, 1811–1831.
- Carey, L. D., M. J. Murphy, T. L. McCormick, and N. W. S. Demetriades (2005), Lightning location relative to storm structure in a leading-line, trailing-stratiform mesoscale convective system, *J. Geophys. Res.*, *110*, D03105, doi:10.1029/2003JD004371.
- Cecil, D. J., S. J. Goodman, D. J. Boccippio, E. J. Zipser, and S. W. Nesbitt (2005), Three years of TRMM precipitation features. Part i: Radar, radiometric, and lightning characteristics, *Mon. Weather Rev.*, *133*, 543–566.
- Chauzy, S., M. Chong, A. Delannoy, and S. Despiau (1985), The June 22 tropical squall line observed during COPT81 experiment: Electrical signature associated with dynamical structure and precipitation, *J. Geophys. Res.*, *90*, 6091–6098.
- Colle, B. A., J. B. Wolfe, W. J. Steenburgh, D. E. Kingsmill, J. W. Cox, and J. C. Shafer (2005), High-resolution simulations and microphysical validation of an orographic precipitation event over the Wasatch mountains during IPEX IOP3, *Mon. Weather Rev.*, *133*, 2947–2971.
- Cuxart, J., P. Bougeault, and J.-L. Redelsperger (2000), A turbulence scheme for mesoscale and large-eddy simulations, *Q. J. R. Meteorol. Soc.*, *126*, 1–30.
- Dash, J., B. L. Mason, and J. S. Wettlaufer (2001), Theory of charge and mass transfer in ice-ice collisions, *J. Geophys. Res.*, *106*, 20,395–20,402.
- Dye, J. E., C. A. Knight, V. Touthenhoofd, and T. W. Cannon (1974), The mechanism of precipitation formation in northeastern Colorado cumulus III. Coordinated microphysical and radar observations and summary, *J. Atmos. Sci.*, *31*, 2152–2159.
- Dye, J. E., J. J. Jones, W. P. Winn, T. A. Cerni, B. Gardiner, D. Lamb, R. L. Pitter, J. Hallett, and C. P. R. Saunders (1986), Early electrification and precipitation development in a small, isolated Montana cumulonimbus, *J. Geophys. Res.*, *91*, 1231–1247.
- Helsdon, J. H., and R. D. Farley (1987), A numerical modeling study of a Montana thunderstorm: Part 2: Model results versus observations involving electrical aspects, *J. Geophys. Res.*, *92*, 5661–5675.
- Helsdon, J. H., W. A. Wojcik, and R. D. Farley (2001), An examination of thunderstorm-charging mechanism using a two-dimensional storm electrification model, *J. Geophys. Res.*, *106*, 1165–1192.
- Jayarathne, R., C. P. R. Saunders, and J. Hallett (1983), Laboratory studies of the charging of soft hail during ice crystal interactions, *Q. J. R. Meteorol. Soc.*, *103*, 609–630.
- Kasemir, H. W. (1960), A contribution to the electrostatic theory of a lightning discharge, *J. Geophys. Res.*, *65*, 1873–1878.
- Kasemir, H. W. (1983), Static discharge and triggered lightning, paper presented at 8th International Aerospace and Ground Conference on Lightning and Static Electricity, Natl. Interagency Coord. Group, Fort Worth, Tex.
- Krehbiel, P., R. J. Thomas, W. Rison, T. Hamlin, J. Harlin, and M. Davis (2000), Lightning mapping observations in Central Oklahoma, *Eos Trans. AGU*, *81*(3), 21–25.
- Lafore, J., et al. (1998), The Meso-NH atmospheric simulation system. Part I: Adiabatic formulation and control simulations, *Ann. Geophys.*, *16*, 90–109.
- Lang, T. J., and S. A. Rutledge (2002), Relationships between convective storm kinematics, precipitation, and lightning, *Mon. Weather Rev.*, *130*, 2492–2506.
- Lang, T. J., et al. (2004), The severe thunderstorm electrification and precipitation study, *Bull. Am. Meteorol. Soc.*, *85*, 1107–1125.
- Lascaux, F., E. Richard, and J.-P. Pinty (2006), Numerical simulations of three MAP IOPs and the associated microphysical processes, *Q. J. R. Meteorol. Soc.*, *132*, 1907–1926, doi:10.1256/qj.05.197.
- Leary, C. A., and R. A. Houze (1979), Melting and evaporating of hydrometeors in precipitation from the anvil clouds of deep tropical convection, *J. Atmos. Sci.*, *36*, 669–679.
- Livingston, J. M., and E. P. Krider (1978), Electric fields produced by Florida thunderstorms, *J. Geophys. Res.*, *83*, 385–401.
- MacGorman, D. R., and D. W. Burgess (1994), Positive cloud-to-ground lightning in tornadic storms and hailstorms, *Mon. Weather Rev.*, *122*, 1671–1697.
- MacGorman, D. R., J. M. Straka, and C. L. Ziegler (2001), A lightning parameterization for numerical cloud model, *J. Appl. Meteorol.*, *40*, 459–478.
- MacGorman, D. R., W. D. Rust, P. Krehbiel, W. Rison, E. Bruning, and K. Wiens (2005), The electrical structure of two supercell storms during STEPS, *Mon. Weather Rev.*, *133*, 2583–2607.
- Mansell, E., D. R. MacGorman, C. L. Ziegler, and J. M. Straka (2005), Charge structure and lightning sensitivity in a simulated multicell thunderstorm, *J. Geophys. Res.*, *110*, D12101, doi:10.1029/2004JD005287.
- Mansell, E. R., D. MacGorman, C. L. Ziegler, and J. M. Straka (2002), Simulated three-dimensional branched lightning in a numerical thunderstorm model, *J. Geophys. Res.*, *107*(D9), 4075, doi:10.1029/2000JD000244.
- Marshall, T. C., M. P. MacCarthy, and W. D. Rust (1995), Electric field magnitudes and lightning initiation in thunderstorms, *J. Geophys. Res.*, *100*, 7097–7103.
- Marshall, T. C., M. Stolzenburg, W. D. Rust, E. R. Williams, and R. Boldi (2001), Positive charge in the stratiform cloud of a mesoscale convective system, *J. Geophys. Res.*, *106*, 1157–1163.
- Nelson, J., and M. B. Baker (2003), Charging of ice-vapor interfaces: Applications to thunderstorms, *Atmos. Chem. Phys.*, *3*, 1237–1252.
- Niemeyer, L., L. Pietronero, and H. J. Wiesmann (1984), Fractal dimension of dielectric breakdown, *Phys. Rev. Lett.*, *52*, 1033–1036.
- Parker, M. D., and R. H. Johnson (2001), Organized modes of midlatitude mesoscale convective systems, *Mon. Weather Rev.*, *128*, 3414–3436.
- Pereyra, R. G., E. E. Avila, N. E. Castellano, and C. P. R. Saunders (2000), A laboratory study of graupel charging, *J. Geophys. Res.*, *105*, 20,803–20,812.
- Prigent, C., E. Defer, J. R. Pardo, C. Pearl, W. B. Rossow, and J. P. Pinty (2005), Relations of polarized scattering signatures observed by the TRMM Microwave Instrument with electrical processes in cloud systems, *Geophys. Res. Lett.*, *32*, L04810, doi:10.1029/2004GL022225.
- Rison, W., R. J. Thomas, P. R. Krehbiel, T. Hamlin, and J. Harlin (1999), A GPS-based three-dimensional lightning mapping system: initial observations in Central New-Mexico, *Geophys. Res. Lett.*, *26*, 3573–3576.
- Rust, W. D., and D. R. MacGorman (2002), Possibly inverted-polarity electrical structures in thunderstorms during STEPS, *Geophys. Res. Lett.*, *29*(12), 1571, doi:10.1029/2001GL014303.
- Rust, W. D., D. R. MacGorman, E. C. Bruning, S. A. Weiss, P. R. Krehbiel, R. J. Thomas, W. Rison, T. Hamlin, and J. Harlin (2005), Inverted-polarity electrical structures in thunderstorms in the Severe Thunderstorm Electrification and Precipitation Study (STEPS), *Atmos. Res.*, *76*, 247–271.
- Rutledge, S. A., and D. R. MacGorman (1988), Cloud-to-ground lightning activity in the 10–11 June 1985 mesoscale system observed during the Oklahoma-Kansas PRE-STORM Project, *Mon. Weather Rev.*, *116*, 1393–1408.
- Rutledge, S. A., C. Lu, and D. R. MacGorman (1990), Positive cloud-to-ground activity in mesoscale convective systems, *J. Atmos. Sci.*, *57*, 2085–2100.

- Saunders, C. P. R., and S. L. Peck (1998), Laboratory studies of the influence of the rime accretion rate on charge transfer during crystal/graupel collisions, *J. Geophys. Res.*, *103*, 13,949–13,956.
- Saunders, C. P. R., W. D. Keith, and R. P. Mitzeva (1991), The effect of liquid water on thunderstorm charging, *J. Geophys. Res.*, *96*, 11,007–11,017.
- Schuur, T. J., and S. A. Rutledge (2000), Electrification of stratiform regions in mesoscale convective systems. Part II: Two-dimensional numerical model simulations of a symmetric MCS, *J. Atmos. Sci.*, *57*, 1983–2006.
- Schuur, T. J., B. F. Smull, W. D. Rust, and T. C. Marshall (1991), Electrical and kinematic structure of the stratiform precipitation region trailing an Oklahoma squall line, *J. Atmos. Sci.*, *48*, 825–842.
- Shao, X. M., and P. R. Krehbiel (1996), The spatial and temporal development of intracloud lightning, *J. Geophys. Res.*, *101*, 26,641–26,668.
- Stoelinga, M. T., et al. (2003), Improvement of microphysical parameterization through observational verification experiment, *Bull. Am. Meteorol. Soc.*, *84*, 1807–1826.
- Stolzenburg, M., T. C. Marshall, W. D. Rust, and B. F. Smull (1994), Horizontal distribution of electrical and meteorological conditions across the stratiform region of a mesoscale convective system, *Mon. Weather Rev.*, *122*, 1777–1797.
- Stolzenburg, M., W. D. Rust, and T. C. Marshall (1998a), Electrical structure in thunderstorm convective regions: 1. Mesoscale convective systems, *J. Geophys. Res.*, *103*, 14,059–14,078.
- Stolzenburg, M., W. D. Rust, and T. C. Marshall (1998b), Electrical structure in thunderstorm convective regions: 2. Isolated storms, *J. Geophys. Res.*, *103*, 14,079–14,096.
- Stolzenburg, M., W. D. Rust, and T. C. Marshall (1998c), Electrical structure in thunderstorm convective regions: 3. Synthesis, *J. Geophys. Res.*, *103*, 14,097–14,108.
- Takahashi, T. (1978), Riming electrification as a charge generation mechanism in thunderstorms, *J. Atmos. Sci.*, *35*, 1536–1548.
- Thomas, R. J., P. R. Krehbiel, W. Rison, T. Hamlin, J. Harlin, and D. Shown (2001), Observations of VHF source powers radiated by lightning, *Geophys. Res. Lett.*, *28*, 143–146.
- Toracinta, E. R., D. J. Cecil, E. J. Zipser, and S. W. Nesbitt (2002), Radar, passive microwave, and lightning characteristics of precipitating systems in the Tropics, *Mon. Weather Rev.*, *130*, 802–824.
- Walser, A., D. Lüthi, and C. Schär (2004), Predictability of precipitation in a cloud-resolving model, *Mon. Weather Rev.*, *132*, 560–577.
- Weisman, M. L., and J. B. Klemp (1984), The structure and classification of numerically simulated convective storms in directionally varying wind shear, *Mon. Weather Rev.*, *112*, 2479–2498.
- Wiens, K. C., S. A. Rutledge, and S. A. Tessendorf (2005), The 29 June 2000 supercell observed during STEPS. Part II: Lightning and charge structure, *J. Atmos. Sci.*, *62*, 4151–4177.
- Williams, E. R. (1989), The tripole structure of thunderstorms, *J. Geophys. Res.*, *94*, 13,151–13,167.
- Zajac, B. A., and S. A. Rutledge (2001), Cloud-to-ground lightning activity in the contiguous united states from 1995–1999, *Mon. Weather Rev.*, *129*, 999–1019.
- Ziegler, C. L., and D. R. MacGorman (1994), Observed lightning morphology relative to modeled space charge and electric field distributions in a tornadic storm, *J. Atmos. Sci.*, *51*, 833–851.
- Ziegler, C. L., P. S. Ray, and D. R. MacGorman (1986), Relations of kinematics, microphysics and electrification in an isolated mountain thunderstorm, *J. Atmos. Sci.*, *43*, 2098–2115.
- Ziegler, C. L., D. R. MacGorman, J. E. Dye, and P. S. Ray (1991), A model evaluation of noninductive graupel-ice charging in the early electrification of a mountain thunderstorm, *J. Geophys. Res.*, *96*, 12,833–12,855.
- Zipser, E. J., and K. R. Lutz (1994), The vertical profile of radar reflectivity of convective cells: a strong indicator of storm intensity and lightning probability?, *Mon. Weather Rev.*, *122*, 1751–1759.
- Zrnić, D. S., N. Balakrishnan, C. L. Ziegler, V. N. Bringi, K. Aydin, and T. Matejka (1993), Polarimetric signatures in the stratiform region of a mesoscale convective system, *J. Appl. Meteorol.*, *32*, 678–693.

C. Barthe and J.-P. Pinty, Laboratoire d'Aérodynamique, Observatoire Midi-Pyrénées, 14 avenue Edouard Belin, F-31400 Toulouse, France. (barc@aero.obs-mip.fr; pinjp@aero.obs-mip.fr)